

Linearly Multiplexed Photon Number Resolving Single-photon Detectors Array

Leonardo Limongi^{a,b}, Francesco Martini^c, Thu Ha Dao^{d,e}, Alessandro Gaggero^c, Hamza Hasnaoui^a, Igor Lopez-Gonzalez^{a,b}, Fabio Chiarello^c, Fabio De Matteis^{d,e}, Alberto Quaranta^{a,f}, Andrea Salamon^e, Francesco Mattioli^c, Martino Bernard^b, Mirko Lobino^{a,f}

^aDepartment of Industrial Engineering, University of Trento, Via Sommarive 9, Povo, 38123, Trento, Italy

^bCenter for Sensors and Devices, Bruno Kessler Foundation, Via Sommarive 18, Povo, 38123, Trento, Italy

^cIstituto di Fotonica e Nanotecnologie, CNR-IFN, Via del Fosso del Cavaliere 100, 00133, Roma, Italy

^dDepartment of Industrial Engineering, University of Rome Tor Vergata, Via del Politecnico 1, 00133, Roma, Italy

^eIstituto Nazionale di Fisica Nucleare, Sezione di Roma Tor Vergata, Via della Ricerca Scientifica, 00133, Roma, Italy

^fINFN TIFPA, Trento Institute for Fundamental Physics and Applications, Via Sommarive 14, Povo, 38123, Trento, Italy

Abstract

Photon Number Resolving Detectors (PNRDs) are devices capable of measuring the number of photons present in an incident optical beam, enabling light sources to be measured and characterized at the quantum level. In this paper, we explore the performance and design considerations of a linearly multiplexed photon number-resolving single-photon detector array, integrated on a single mode waveguide. Our investigation focus on defining and analyzing the fidelity of such an array under various conditions and proposing practical designs for its implementation. Through theoretical analysis and numerical simulations, we show how propagation losses and dark counts may have a strong impact on the performance of the system and highlight the importance of mitigating these effects in practical implementations.

Keywords: Photon Number Resolving Detector, Single-photon Detector, Superconducting Nanowire Single-photon Detector, Lithium Niobate-on-Insulator, Niobium Nitride, Photonic Integrated Circuit, Photonic chip

1. Introduction

Photon Number Resolving Detectors (PNRDs) are devices capable of measuring the number of quanta of energy present in an incident optical field, enabling light sources to be measured and characterized at the quantum level [1, 2, 3]. PNRDs have a pivotal role in various optical applications and quantum technologies. In quantum key distribution [4], PNRDs can be used in specific protocols [5] to guarantee secure transmission of information. In quantum imaging, they enable high-resolution by precisely counting the photons emitted or scattered by objects of interest [6]. Moreover, they can be used in other applications such as quantum state preparation [7, 8], photon-counting Lidar [9], quantum metrology [10], and quantum tomography [11].

Photon Number Resolving Detectors can be realized with different technologies, each one with its characteristics, operating principles, and limitations. For instance, schemes with photomultiplier tubes [12] and Geiger-mode avalanche photodiodes (GAPDs) [13] have shown photon number resolution with few photons. Visible light photon counters [14] have a high dark count rate and slow operational rate, while transition edge sensors (TES) can discriminate the number of photons with high efficiency (98%) [15] and low noise at telecommunication wavelengths, but their performance is limited by the low count rates and high time jitter [16, 17].

Superconducting Nanowire single photon detector (SNSPD) [18] is considered one of the most promising platform for overcoming the limitations of the detector platforms mentioned above, thanks to its high efficiency [19], negligible dark count

rate [20], jitter time in the picosecond region, [21] and short recovery time [22]. However, single SNSPD detectors do not have intrinsic photon number resolution capability like TES detectors. Here we show how this limit can be addressed with a multiplexed scheme on an optical waveguide to enable photon number resolution and optimized fidelity.

Integration of SNSPD detectors on optical waveguide chips has been demonstrated, showing how these devices maintain their outstanding properties for a diverse range of materials [23]. Integration with complex photonic waveguide networks has shown the possibility of creating a combined platform which contains both capabilities of SNSPDS and PNRDs with great scalability potential [24, 25, 26, 27, 28] and applications in quantum communication [29], characterization of quantum photon statistics [25] and quantum sensing [30].

Here we propose a design for a linearly multiplexed PNRD based on SNSPD, integrated on a single optical waveguide. First, keeping generality, we show the theoretical calculations of each element efficiency to maximize the fidelity, accounting for waveguide losses and dark counts. Then, a design is proposed, showing a guideline to obtain optimized parameters considering fabrication constraints. For our design we focus on silicon nitride strip loaded waveguide on a thin film lithium niobate (TFLN) substrate [31] as photonic platform because it offers the great potential of TFLN in terms of nonlinearity and electrooptical reconfigurability, but it is more agile to fabricate as it exploits the well established manufacturing techniques for silicon nitride leaving the hard-to-process LN film intact.

This proposal aims at the integration of PNR capability in

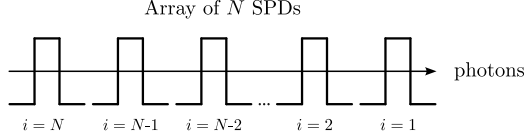


Figure 1: Photon-number resolving detector array geometry: photons travel from left to right through a series of N single-photon detectors, indexed from N to 1.

a photonic integrated circuit (PIC) that, thanks to TFLN properties, can exploit the nonlinear properties of lithium niobate to generate and manipulate quantum states of light [32] on a single chip. Moreover, due to its linearity, our design can be considered modular in the sense that SPD elements can be added to the detector array incrementally.

The manuscript is structured as follows: In Sect. 2 we will discuss a general approach for the geometry of an array of SNSPDs on a linear waveguide and calculate the relevant merit factors in the case of ideal waveguide and detectors. Then, non-idealities such as propagation losses and detector dark counts will be discussed and estimated. In Sect. 3 an actual design for the implementation of the waveguide PNRD will be proposed and discussed. Simulations will be used to calculate the relevant parameters for the proposed device so that the final merit factors can be calculated using the theory developed in Sect. 2. In Section IV we will summarize the results and draw our conclusions.

2. A multiplexed SNSPDs on a single waveguide

2.1. Lossless waveguide and detector

First, we consider the ideal case of an array of N single-photon detectors (SPDs) coupled to a lossless waveguide, with no dark counts, and schematically shown in Fig.1. Each element of the array works in the Geiger mode and can only discriminate between light and no light, generating the same signal for any number of absorbed photons. The detectors are numbered so that the first element to be illuminated has index N and the last is element 1. The fidelity F in this ideal system as a function of the number of incoming photons m and the number of SPDs N is given by the probability of correctly detecting all of the m incoming photons, expressed as

$$F = p(\text{detected} = m | \text{incoming} = m). \quad (1)$$

The probability in Eq. 1 can be reinterpreted as the probability that each element of our array absorbs and detects either zero or one photon and no photon is lost at the end of the array.

To derive its expression, consider N SPDs arranged linearly as depicted in Fig. 1 and let $\mathcal{D} = \{i\}_{i=1}^N$ denote the ordered set of detector indices with the value N associated to the first detector illuminated and 1 to the last. Define $\mathcal{F} \subset \wp(\mathcal{D})$ as the family of sets containing m elements in the power set of \mathcal{D} , representing all possible combinations of m different detectors detecting the m incoming photons. Recall that the power set of \mathcal{D} is the set

of all subsets of \mathcal{D} , namely

$$\begin{aligned} \wp(\mathcal{D}) &= \{\mathcal{S} \mid \mathcal{S} \subseteq \mathcal{D}\} = \\ &= \{\emptyset, \{1\}, \{2\}, \dots, \{N\}, \{1, 2\}, \{1, 3\}, \dots, \\ &\quad \{N-1, N\}, \dots, \{1, 2, \dots, N\}\} \end{aligned}$$

and that $|\wp(\mathcal{D})| = 2^N$ is the number of elements inside $\wp(\mathcal{D})$. Hence, \mathcal{F} can be expressed as

$$\begin{aligned} \mathcal{F} &= \{\mathcal{S} \in \wp(\mathcal{D}) \mid |\mathcal{S}| = m\} = \\ &= \{\{1, 2, \dots, m-1, m\}, \{1, 2, \dots, m-1, m+1\}, \dots, \\ &\quad \{N-m, N-m+1, \dots, N\}\} \end{aligned}$$

which contains $\binom{N}{m} = \frac{N!}{m!(N-m)!}$ elements, or m -dimensional vectors denoted as \vec{k} equivalently, identifying every possible choice of m indices out of the total N of detectors. It is important to notice that \mathcal{F} contains every possible list of SPDs that have detected one photon with the constraint of both no photon losses and at most one photon per SPD.

Now, denote η_i as the efficiency of the i -th detector to click when illuminated with a single photon, we can write the probability of a photon being absorbed by the i -th element of the array as

$$p_i = \eta_i \prod_{j=i+1}^{N+1} (1 - \eta_j) \quad (2)$$

where $\eta_{N+1} = 0$, representing free propagation before entering the array, and the product $\prod_{j=i+1}^{N+1} (1 - \eta_j)$ indicates the probability of a photon not being absorbed before the i -th detector.

Under these assumptions, the probability of distributing at most one of the m incoming photons over the N SPDs, or equivalently the fidelity of the PNR detector, is given by

$$F(m, N) = \sum_{\vec{k} \in \mathcal{F}} m! \prod_{k_i \in \vec{k}} \eta_{k_i} \prod_{j=k_i+1}^{N+1} (1 - \eta_j) \quad (3)$$

where $m!$ accounts for all permutations of the photons inside each \vec{k} vector.

When there are m incoming photons, the maximum fidelity is obtained when the probability of absorbing a single photon is uniform across each element of the array [33] and is given by

$$p_i = \frac{1}{N} \quad \forall i \in [1, N]. \quad (4)$$

Substituting Eq. 4 in Eq. 2, the efficiency of the i -th element of the array is given by

$$\eta_i = \frac{1}{i} \quad \text{with } 1 \leq i \leq N \quad (5)$$

Equation 5 implies that the first detector of the array will have the smallest efficiency of $1/N$ while the last one requires total absorption ($\eta=1$) for preventing light from escaping the array, corresponding to a nanowire of infinite length. Combining this

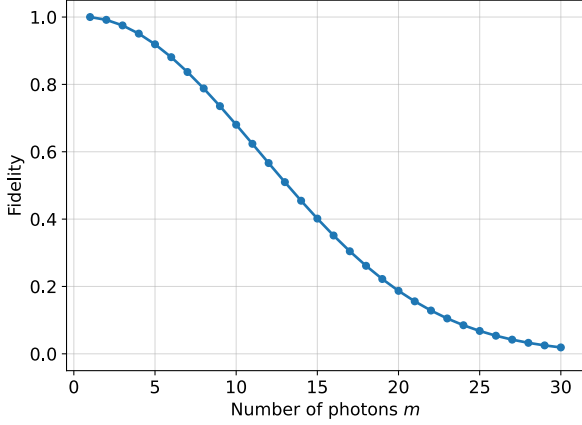


Figure 2: Fidelity versus the number of incoming photons m (blue points) with $N = 120$ single-photon detectors. This plot was obtained by a second order Stirling expansion of Eq. 6.

result with Eq. 3, we obtain a maximum fidelity for the detection of m photons with an array of N detectors of

$$F(m, N) = m! \binom{N}{m} \frac{1}{N^m}. \quad (6)$$

It is worth to note that the same result is obtained in [34] by starting from the same assumptions. The fidelity of Eq. 6 is shown in Fig. 2 for an array of $N = 120$ elements, and it represents the ideal case in which we considered only dichotomous events of photons being either absorbed or not.

2.2. Propagation losses and fidelity

All real waveguide suffers from propagation losses, and in this situation Eq. 6 is not valid. In this case the ratio between the losses introduced by the waveguides and the absorption of the SPDs plays a fundamental role for the calculation of the fidelity.

Consider a waveguide with a loss coefficient α_w , and a superconducting nanowire with absorption coefficient α_c . As the mechanisms are the same for both the elements, the probability of a photon being absorbed or not over a distance L is given by:

$$\mathcal{A} = 1 - e^{-\alpha L}, \quad \mathcal{T} = 1 - \mathcal{A} = e^{-\alpha L} \quad (7)$$

where \mathcal{A} and \mathcal{T} are, respectively, the absorption and the transmission probabilities, both governed by the coefficient α . For the i -th element of the array Eq. 5 holds and we have $\mathcal{A}_i = \eta_i = 1/i$, from where we can extract the length of the element by inverting the first of Eqs. 7 with absorption coefficient α_c , namely

$$L_i = \frac{1}{\alpha_c} \ln\left(\frac{1}{1 - \mathcal{A}_i}\right) = \frac{1}{\alpha_c} \ln\left(\frac{i}{i-1}\right). \quad (8)$$

To incorporate propagation losses into the fidelity computation, we modify Eq. 2 for the probability of a photon being absorbed by the i -th detector as follows

$$p_i = \mathcal{A}_i^{(nw)} \prod_{j=i+1}^{N+1} \mathcal{T}_j^{(nw)} \mathcal{T}_j^{(wg)} \quad (9)$$

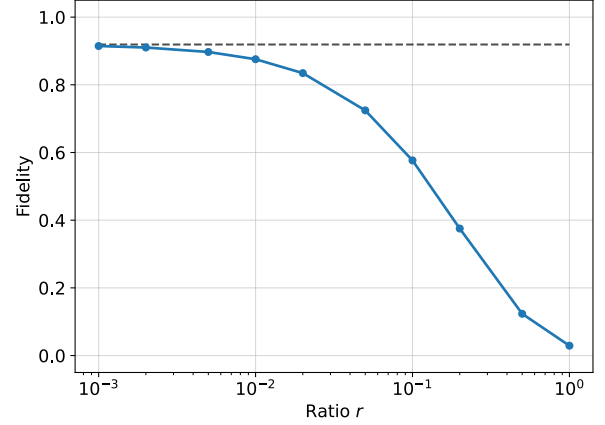


Figure 3: Fidelity with propagation losses versus the ratio $r = \alpha_w/\alpha_c$ (blue points - Lossy) with $N = 120$ single-photon detectors and $m = 5$ incoming photons. For an increasing r the fidelity drops from the lossless of 0.9191 (black dashed line) to zero in a monotonic and continuous way.

where we assume photons to survive both the waveguides (wg) and the nanowires (nw) until before the i -th element and being absorbed by it.

Substituting Eq. 9 into Eq. 3, and leveraging Eqs. 7 and 8, we derive the following loss-perturbed fidelity expression

$$F(m, N, r) = m! \left(\frac{1}{N}\right)^{m(r+1)} \sum_{\vec{k} \in \mathcal{F}} \prod_{k_i \in \vec{k}} k_i^r \quad (10)$$

where $r = \alpha_w/\alpha_c$ represents the ratio of the absorption coefficients of the waveguide and the nanowire detector.

Figure 3 shows how fidelity changes with respect to r when we send 5 photons into an array of 120 detectors, each with length given by Eq 8.

2.3. Detector with dark counts

Next we introduce detectors dark counts in our calculation assuming a dark count rate (DCR) per unit time proportional to the length of the nanowire [35]. For an array of N detectors where the length of each element is given by Eq. 8, the total length L_{tot} is

$$L_{\text{tot}} = L_1 + \sum_{i=2}^N L_i = L_1 + \frac{1}{\alpha_c} \ln N, \quad (11)$$

where we isolated the divergent term for $i = 1$ because in the ideal case the last detector absorbs 100% of the photons and have infinite length.

We assume a $\text{DCR} = L_{\text{tot}}\gamma$, where γ is a coefficient that depends on the properties of the superconducting nanowire. The probability of having k dark counts in a time interval Δt follows the Poisson distribution

$$p(k, \Delta t) = \frac{(L_{\text{tot}}\gamma\Delta t)^k}{k!} e^{-(L_{\text{tot}}\gamma\Delta t)} \quad (12)$$

The probability of having no dark counts for the measurement time Δt is given by $p(0, \Delta t)$, and hence we can multiply it

to Eq. 10 to obtain the loss-DCR-perturbed fidelity

$$F(m, N, r, \gamma \Delta t) = m! \left(\frac{1}{N} \right)^{m(r+1)} N^{-\frac{\gamma \Delta t}{\alpha c}} e^{-\gamma \Delta t L_1} \sum_{\vec{k} \in \mathcal{F}} \prod_{k_i \in \vec{k}} k_i^r \quad (13)$$

For state of the art SNSPDs this correction is usually quite small since the dark count rate can go down to few tens of Hz and the measurement time is of the order of ns [26].

3. Design of the detector array on a strip-loaded waveguide on TFLN

The relations for the fidelity derived in the previous sections can be applied to any material platform for either the waveguide and the nanowire detectors. Now we consider a device fabricated on a lithium niobate on insulator (LNOI) substrate loaded with a Silicon Nitride (Si_3N_4 or SiN) waveguide strip and coupled to a series of Niobium Nitride (NbN) SNSPDs, with the geometry sketched in Fig. 4a. The PNRD is fabricated on a LNOI substrate made by a 300 nm lithium niobate layer on a 3 μm silicon dioxide (SiO_2) insulator. On the LNOI film, a ridge in SiN is patterned with a nominal a width of 1.2 μm and a thickness of 200 nm, defining the waveguide channel. The SNSPDs are then patterned on top of the SiN ridge with a fixed thickness of 6 nm and a width of 80 nm. Such series of SNSPDs can be realized on top of the strip-loaded LNOI photonic circuit thanks to the following fabrication steps. A SiO_2 cladding layer is deposited by Plasma-Enhanced Chemical Vapor Deposition, and a planarization step is performed by Chemical Mechanical Polishing (CMP). The NbN superconducting film is deposited using DC Magnetron Sputtering, and the different nanowire patterns are realized by Electron Beam Lithography followed by dry etching. AuPd resistors, placed in parallel to each nanowire element, and Au contact pads are fabricated via lift-off. Such fabrication procedure is the same employed in [36], except for the CMP step that allows to position both the contact pads and AuPd parallel resistors on the cladding layer. In addition, such step grants optimal surface roughness prior the SNSPD fabrication.

Such a structure is simulated using the finite elements method (FEM) with the parameters summarized in Tab. 1.

3.1. Straight and curved propagation

Initially, to estimate the propagation losses in passive structures, and determine α_w , FEM simulations were conducted for strip-loaded waveguides, excluding the NbN layer, for both straight and curved configurations.

For the first part of simulations, we performed a parametric sweep varying both the SiN waveguide width and height to take into account different fabrication scenarios. The waveguide height ranged from 180 to 220 nm, while the width varied between 1 μm and 1.4 μm . For a thickness of 200 nm and a width of 1.2 μm , we obtained a single mode waveguide with an effective refractive index $n_{\text{eff}} = 1.8066$.

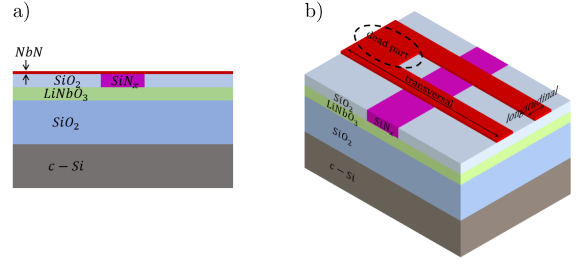


Figure 4: Cross sections of the photon-number resolving detector: starting from the bottom there are a crystalline silicon (c-Si) layer, a silicon oxide (SiO_2) layer, a lithium niobate (LiNbO_3) layer, a silicon nitride (SiN_x) waveguide surrounded by an SiO_2 layer, and finally the niobium nitride (NbN) layer. The detailed dimensions are reported in Tab.1.

$\lambda = 1.55 \mu\text{m}$	SiO_2	LiNbO_3	Si_3N_4	NbN
Refractive index n	1.44	2.21(o) 2.14(e)	1.88	5.23+ i5.82
Thickness h (μm)	3.00	0.3	0.2	0.006
Width (μm)	slab	slab	1.20	0.08

Table 1: List of parameters used for the FEM simulations. Both SiO_2 and SiN refractive index are obtained by Variable Angle Spectroscopic Ellipsometry measurements on fabricated samples. LiNbO_3 and NbN refractive index are respectively reported in [37] and [38].

After determining the single mode n_{eff} under ideal conditions, we looked at the stability of such waveguides with respect to slab leakages. The latter can be characterized by the difference in the effective refractive index between strip-loaded and slab modes [39], denoted as $\Delta n = n_{\text{eff}}^{(\text{strip})} - n_{\text{eff}}^{(\text{slab})}$. Following the last reference, a simple way to see whether or not lateral leakage occurs, is to study the sign of Δn . Indeed, strip-loaded waveguides suffer from strong lateral leakage when $\Delta n < 0$.

For this purpose, we modified the simulation setup by removing the SiN waveguide layer, leaving only the LN slab with an additional oxide layer on top. To ensure comparability with previous results, we conducted a parametric sweep on the thickness of the oxide layer using the same values as in the strip-loaded waveguide simulations. In our scenario, both TE and TM polarizations of the slab modes exhibit effective refractive indices ($n_{\text{eff}}^{(\text{slab,TE})} = 1.7714$ and $n_{\text{eff}}^{(\text{slab,TM})} = 1.6070$ respectively) lower than that of the strip-loaded TE mode, thus providing robust mode isolation during straight propagation with respect to lateral leakages.

In curved waveguides, radiative leakage rises sharply when the bending radius R is sufficiently small. To assess this possibility and determine the critical bending radius R_{crit} at which radiative losses become significant, we conducted FEM simulations of a strip-loaded ring resonator. Maintaining constant waveguide thickness and width, we evaluated the quality factor of the ring as a function of its radius, ranging from 40 μm to

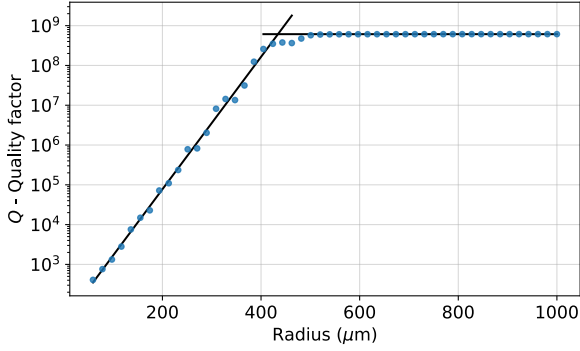


Figure 5: Log-scale plot of the quality factor of the simulated ring resonator as a function of the radius. The blue points represent the simulation results, while the black lines are the fit for both horizontal behaviors, that saturates at $Q_{\infty} = 6.11 \cdot 10^8$, and the slope. The latter has a value of $1.66 \cdot 10^{-1}$ dB/ μm and it indicates how much the quality factor's order of magnitude changes with respect to the bending radius. The intersection of the fits is at $R = 434 \mu\text{m}$, representing the radius under which the bending radiative losses are the dominating factor.

1 mm. These results are shown in Fig. 5 which exhibits two distinct regions. First, for small radii, there is an exponential decay of the ring quality factor with decreasing radii which indicates that radiative losses dominate over other loss mechanisms. In the second region, for larger radii, we see a saturation of the ring quality factor to a value of $6.11 \cdot 10^8$ which suggests that bend-related radiative losses become negligible beyond a certain radius. The remaining sources of losses could be either physical, such as substrate losses or scattering due to the waveguide roughness, or non-physical, for example due to artifacts of the simulation such as the finite size of the simulation window.

From the intersection of the linear fits (on the y-log scale) of the data in Fig. 5, we estimate a critical radius $R_{\text{crit}}=434 \mu\text{m}$. Below R_{crit} where radiative losses dominate, the slope of the fit is $0.166 \frac{\text{dB}}{\mu\text{m}}$ and indicates the quality factor's order of magnitude variation with respect to the variation of the bending radius.

3.2. Tuning SPDs efficiency

The geometry of NbN nanowires along the waveguide is a key aspect for designing a good PNRD. Figure 6 reports a summary of the geometry we investigated. Advantages and drawbacks of each configuration are discussed in this section.

As stated in the previous sections, the absorption efficiency of a nanowire can be tuned by its interaction length with the mode of the waveguide. For such a purpose, disposing the nanowire parallel to the waveguide, as showed in Fig. 6a, could be the best solution for the fabrication of efficiency-tunable NbN SPDs. Indeed, our simulations show that a nanowire in such a configuration absorbs $\alpha_c = 422 \frac{\text{dB}}{\text{cm}}$, while SiN strip-loaded LNOI waveguides can reach propagation losses as low as $\alpha_w = 0.3 \frac{\text{dB}}{\text{cm}}$ [40]. This number translates into a ratio $r < 10^{-3}$ and a fidelity close to the ideal case as shown in Fig. 3. Additionally, one can estimate the probability of having zero dark counts per measurement (Eq. 12) as follows: suppose $N = 120$ SPDs in the array, the worst scenario reported in [26] suggests considering $\text{DCR} = 30k \text{ Hz}$ for a $60 \mu\text{m}$ nanowire, the measurement time can be taken as $t = 10 \text{ ns}$ as it shall not be

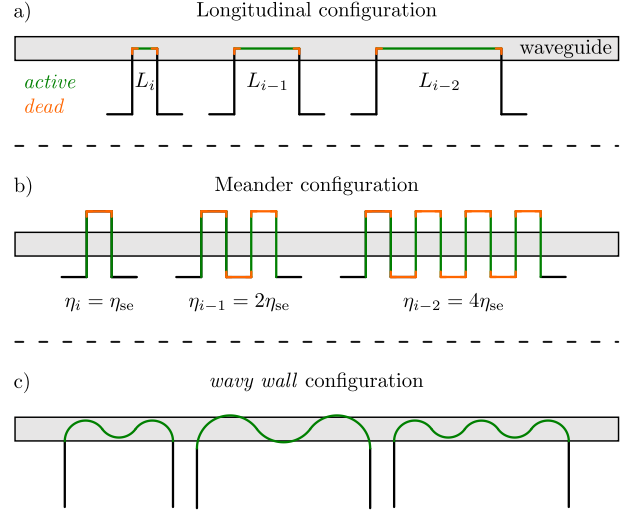


Figure 6: Different disposition of the NbN nanowire along the waveguide with highlighted *active* and *dead* parts respectively in orange and green colors. Panel a) shows the longitudinal configuration, characterized by having the detecting NbN nanowire parallel to the waveguide, and the detection efficiency can be continuously tuned by varying the nanowire's length L_i . Panel b) shows the meander configuration, characterizing by the detecting nanowire being perpendicular to the waveguide. Here the efficiency is discretized, and can be selected only among multiples of the single-element efficiency η_{se} . Panel c) shows the *wavy wall* configuration, being characterized by having the active part of the nanowire in a periodic and uniform-curvature shape. Specifically, each SPD is formed by circumference arcs with fixed radius.

less than the latching time of SNSPDs [41], and we chose to have the last SPD in the array - the one indexed $i = 1$ - to be 50% absorptive as the second-last so that $L_1 = L_2 = \frac{1}{\alpha_c} \ln 2$. With such hypothesis we obtain a probability of having no dark counts per measurement in the worst DCR scenario of $p(0, 10 \text{ ns}) \approx 0.9972$.

Despite its flexibility, this configuration poses challenges in bending the nanowires over the waveguide. Indeed, curved nanowires often lead to current crowding issues [42], making straight sections practically ineffective. To mitigate this occurrence, widening the nanowire in curved sections is a potential solution, but it introduces absorptive *dead* zones atop the waveguide, as noticeable in Fig. 4b, significantly impacting the fidelity.

An alternative approach involves arranging the nanowires transversally to the waveguide in a meander structure, as showed in Fig. 6b. This arrangement places the curved parts of the nanowires farther from the waveguide, significantly reducing the absorption of the *dead* sections. On the other hand, as the SPD-waveguide interaction now occurs over a discrete number of nanowire elements (only those being transversal to the waveguide), the coupling coefficients of the SPDs can only be selected on a *discretized* grid composed by multiples of the single-element efficiency η_{se} , being defined as the absorption given by 2 *active* sections. We neglect the absorption of the *dead* sections as they can be optimized to be negligible, as we will show in the following.

On the basis of pros and cons of longitudinal and meander configurations, and given the results obtained by [42] with a

similar device, we want to discuss a third geometry. As showed in Fig. 6c, one can fabricate the NbN SPD with a curvature maintaining shape, only changing periodically the rotation orientation like a *wavy wall*. In such a way, one can in principle eliminate the current crowding issue, as here the whole nanowire has the same curvature and consequently eliminating *dead* sections, and still being able to tune the efficiency of each NbN in a continuous way. On the other hand, the *wavy wall* nanowire fabrication feasibility could be limited due to resolution constraints and longer processing times, but we strongly believe that it could be beneficial for a better tuning of SPDs efficiencies.

Due to the better ease of the fabrication process, we opt to proceed our study with a PNRD composed of meander SPDs. To evaluate η_{se} , we conducted FEM simulations of both *active* and *passive* regions, sweeping both waveguide height and NbN nanowire transversal length. The latter parameter is the defined as the joint length of *active* and *passive* parts of the nanowire meander, hence comprising a straight section and the curve. The simulation results of this study are represented in Fig. 7 as absorption percentages versus the transversal length. Notably, both regions saturate their absorption over a length of

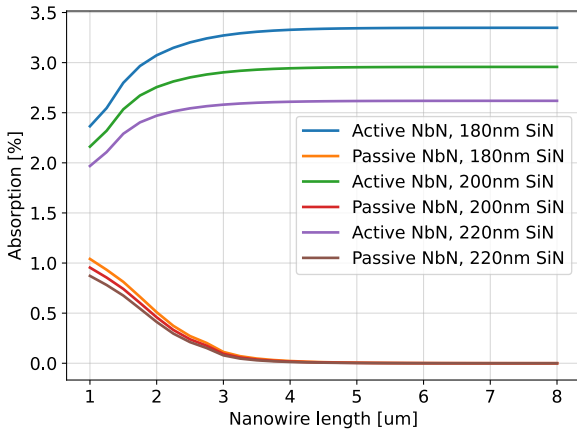


Figure 7: FEM simulation of the absorption as a function of the nanowire length. The latter takes into account both *active* (transversal straight) and *passive* (block for the curve) of a NbN nanowire of fixed 6 nm thickness and 80 nm width. The parametric sweep was performed on three waveguide heights and with nanowire transversal length ranging from 1 μm to 8 μm with 0.25 μm steps.

approximately 5 μm , with the active portion reaching saturation between 2.5 and 3.5%, depending on the SiN thickness, while the dead zone exhibits absorption below $6 \cdot 10^{-3}\%$.

As previously mentioned, the *dead* section of the nanowire can be considered to have negligible absorbance, resulting in a single-element SPD efficiency for a 200 nm thick SiN waveguide of $\eta_{se} = 2.957\%$. To determine the index of the smallest feasible element in the array, we can invert Eq. 5 and solve for N , given by:

$$N = \lfloor 1/\eta_{se} \rfloor \quad (14)$$

where $\lfloor \cdot \rfloor$ denotes the floor function, representing the integer part of the expression. In our implementation, this calculation yields to $N = 33$ SPDs for the PNRD.

The efficiency of the i -th SPD can be discretized using the following equation:

$$\eta_i = 1 - (1 - \eta_{se})^{u_i} \quad (15)$$

where u_i denotes the number of units required to achieve the efficiency η_i using η_{se} . The corresponding u_i values for each SPD can be determined by inverting Eq. 15

$$u_i = \text{round} \frac{\log\left(1 - \frac{1}{\eta_i}\right)}{\log(1 - \eta_{se})} \quad (16)$$

where the round operator is employed because u_i must be an integer.

The values obtained for each i between 1 and 33 are reported in Tab. 2.

index i	u_i	index i	u_i	index i	u_i
33	1	22	2	11	3
32	1	21	2	10	4
31	1	20	2	9	4
30	1	19	2	8	4
29	1	18	2	7	5
28	1	17	2	6	6
27	1	16	2	5	7
26	1	15	2	4	10
25	1	14	2	3	14
24	1	13	3	2	23
23	1	12	3	1	77

Table 2: List of u_i meanders of each SPD

Using these data and the methodologies discussed in Sec. 2 and the worst dark counts scenario in [26] we evaluate the performance of a PNRD composed by $N = 33$ meander SPDs in different regimes: ideal, lossy and lossy plus DC. We then compare these results to the non-discretized ideal scenario by examining the fidelity ratio F_{disc}/F_{ideal} , as shown in Fig. 8: remarkably, the introduction of losses did not change significantly the performance of such PNRD, which the introduction of dark counts did instead.

Finally, we explicitly report the fidelities from 1 to 4 photons of such a detector considering both losses and dark counts: $F(1, 33) = 98.95\%$, $F(2, 33) = 94.87\%$, $F(3, 33) = 88.04\%$ and $F(4, 33) = 79.00\%$.

4. Discussion and conclusions

Performance and design considerations of a linearly multiplexed photon number-resolving single-photon detector array have been discussed. Our investigation focused on analyzing

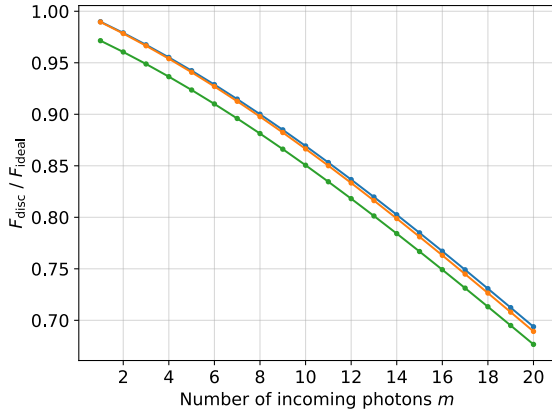


Figure 8: Performance of the discretized array obtained as the discretized fidelity normalized with the ideal fidelity. The three lines represent the different regimes: discretized only (blue line), discretized with propagation losses (orange line) and discretized with both propagation losses and dark count (green line) all considering 33 SPDs in the PNRD. The DC contribution is $p(0, 10 \text{ ns}) = 98.17\%$.

the fidelity of the PNR in detecting m incident photons under various conditions and proposing a practical design for its implementation.

We began by deriving expressions for the fidelity of the SNSPD array, starting from the ideal case and then considering perturbation factors such as propagation losses and dark counts. Through theoretical analysis and numerical simulations, we demonstrated how these factors affect the fidelity of the system.

Moving on to the design aspect, we proposed a strip-loaded waveguide design for the SNSPD array, utilizing LNOI as the platform material. By conducting FEM simulations, we evaluated the performance of a $200 \mu\text{m}$ thick SiN strip loading a $300 \mu\text{m}$ LN slab layer, including straight and curved propagation losses, the latter to understand the limitations of curved designs. We also discussed how to prevent slab-mode leakage in strip-loaded waveguides and showed that it is not an eventuality in our design.

Our investigation revealed important insights into the trade-offs involved in the design of the SNSPD array. We briefly mentioned current crowding in curved nanowires and suggested two different solutions: the longitudinal and the *discretized* ones. We also studied the efficiency of the superconducting NbN nanowire detectors for different lengths and nitride thicknesses. We conclude that the absorption of both *active* and *passive* sections of the nanowires reach their plateau value after about $5 \mu\text{m}$ of length. Additionally, we would like to propose another nanowire configuration, that we called *wavy wall*: here, every SPD is formed by a nanowire that continuously curve along the waveguide, periodically changing the curvature orientation like a sinusoid centered on the waveguide. The advantage of such a configuration is that, in principle, it would not suffer by current crowding as it is formed by a uniform curve.

In conclusion, our study provides valuable insight into the performance and design of linearly multiplexed photon number-resolving single-photon detector arrays. By address-

ing key challenges and proposing practical solutions, we aim to contribute to the advancement of quantum technologies relying on photon detection and quantum state engineering.

Acknowledgements

L.L., F.Mar., T.H.D., A.G., F.C., A.S, F.Mat. and M.B. acknowledge the support of the PNRR MUR project PE0000023-NQSTI (Italy).

This work was funded by INFN through the CSN5-UNIDET project.

References

- [1] M. von Helversen, J. Böhm, M. Schmidt, M. Gschrey, J.-H. Schulze, A. Strittmatter, S. Rodt, J. Beyer, T. Heindel, S. Reitzenstein, Quantum metrology of solid-state single-photon sources using photon-number-resolving detectors, *New Journal of Physics* 21 (2019) 035007. doi:10.1088/1367-2630/ab0609.
- [2] L. Stasi, P. Caspar, T. Brydges, H. Zbinden, F. Bussi eres, R. Thew, High-efficiency photon-number-resolving detector for improving heralded single-photon sources, *Quantum Science and Technology* 8 (2023) 045006. doi:10.1088/2058-9565/ace54b. arXiv:2210.16005.
- [3] R. H. Hadfield, M. J. Stevens, S. S. Gruber, A. J. Miller, R. E. Schwall, R. P. Mirin, S. W. Nam, Single photon source characterization with a superconducting single photon detector, *Optics Express* 13 (2005) 10846. doi:10.1364/OPEX.13.010846. arXiv:quant-ph/0511030.
- [4] F. Xu, X. Ma, Q. Zhang, H.-K. Lo, J.-W. Pan, Secure quantum key distribution with realistic devices, *Reviews of Modern Physics* 92 (2020) 025002. doi:10.1103/RevModPhys.92.025002. arXiv:1903.09051.
- [5] M. Cattaneo, M. G. A. Paris, S. Olivares, Hybrid quantum key distribution using coherent states and photon-number-resolving detectors, *Physical Review A* 98 (2018) 012333. doi:10.1103/PhysRevA.98.012333. arXiv:1707.02852.
- [6] O. Wolley, T. Gregory, S. Beer, T. Higuchi, M. Padgett, Quantum imaging with a photon counting camera, *Scientific Reports* 12 (2022) 8286. doi:10.1038/s41598-022-10037-x.
- [7] G. Harder, T. J. Bartley, A. E. Lita, S. W. Nam, T. Gerrits, C. Silberhorn, Single-Mode Parametric-Down-Conversion States with 50 Photons as a Source for Mesoscopic Quantum Optics, *Physical review letters* 116 (2016) 143601. doi:10.1103/PhysRevLett.116.143601. arXiv:1510.05801.
- [8] D. A. Kuts, M. S. Podoshvedov, B. A. Nguyen, S. A. Podoshvedov, Realistic conversion of single-mode squeezed vacuum state to large-amplitude high-fidelity Schrödinger cat states by inefficient photon number resolving detection, *Physica Scripta* 97 (2022) 115002. doi:10.1088/1402-4896/ac955f.
- [9] J. Huang, M. Ren, Y. Liang, Z. Wang, X. Wang, W. Kong, E. Wu, G. Wu, H. Zeng, Photon-counting laser ranging with InGaAs/InP avalanche photodiode in the passively quenched and 1-GHz sinusoidally gated, *Optik* 125 (2014) 3744-3747. doi:10.1016/j.ijleo.2014.01.133.
- [10] J.-Y. Wu, N. Toda, H. F. Hofmann, Quantum enhancement of sensitivity achieved by photon-number-resolving detection in the dark port of a two-path interferometer operating at high intensities, *Physical Review A* 100 (2019) 013814. doi:10.1103/PhysRevA.100.013814. arXiv:1903.11282.
- [11] S. Olivares, A. Allevi, G. Caiazzo, M. G. A. Paris, M. Bondani, Quantum tomography of light states by photon-number-resolving detectors, *New Journal of Physics* 21 (2019) 103045. doi:10.1088/1367-2630/ab4afb. arXiv:1809.00818.
- [12] G. Zambra, M. Bondani, A. S. Spinelli, F. Paleari, A. Andreoni, Counting photoelectrons in the response of a photomultiplier tube to single picosecond light pulses, *Review of Scientific Instruments* 75 (2004) 2762-2765. doi:10.1063/1.1777407.
- [13] J. Blazej, Photon number resolving in Geiger mode avalanche photodiode photon counters, *Journal of Modern Optics* 51 (2004) 1491-1497. doi:10.1080/09500340408235287.

- [14] E. Waks, K. Inoue, W. D. Oliver, E. Diamanti, Y. Yamamoto, High-efficiency photon-number detection for quantum information processing, *IEEE Journal of Selected Topics in Quantum Electronics* 9 (2003) 1502–1511. doi:10.1109/JSTQE.2003.820917. arXiv:quant-ph/0308054.
- [15] D. Fukuda, G. Fujii, T. Numata, K. Amemiya, A. Yoshizawa, H. Tsuchida, H. Fujino, H. Ishii, T. Itatani, S. Inoue, T. Zama, Titanium-based transition-edge photon number resolving detector with 98% detection efficiency with index-matched small-gap fiber coupling, *Optics Express* 19 (2011) 870. doi:10.1364/OE.19.000870.
- [16] A. J. Miller, S. W. Nam, J. M. Martinis, A. V. Sergienko, Demonstration of a low-noise near-infrared photon counter with multiphoton discrimination, *Applied Physics Letters* 83 (2003) 791. doi:10.1063/1.1596723.
- [17] A. E. Lita, A. J. Miller, S. W. Nam, Counting near-infrared single-photons with 95% efficiency, *Optics Express* 16 (2008) 3032. doi:10.1364/OE.16.003032.
- [18] C. M. Natarajan, M. G. Tanner, R. H. Hadfield, Superconducting nanowire single-photon detectors: physics and applications, *Superconductor Science and Technology* 25 (2012) 063001. doi:10.1088/0953-2048/25/6/063001.
- [19] D. V. Reddy, R. R. Nerem, S. W. Nam, R. P. Mirin, V. B. Verma, Superconducting nanowire single-photon detectors with 98% system detection efficiency at 1550 nm, *Optica* 7 (2020) 1649. doi:10.1364/OPTICA.400751.
- [20] H. Shibata, K. Shimizu, H. Takesue, Y. Tokura, Ultimate low system dark-count rate for superconducting nanowire single-photon detector, *Optics Letters* 40 (2015) 3428. doi:10.1364/OL.40.003428. arXiv:1507.01743.
- [21] B. Korzh, Q.-Y. Zhao, J. P. Allmaras, S. Frasca, T. M. Autry, E. A. Bersin, A. D. Beyer, R. M. Briggs, B. Bumble, M. Colangelo, G. M. Crouch, A. E. Dane, T. Gerrits, A. E. Lita, F. Marsili, G. Moody, C. Peña, E. Ramirez, J. D. Rezac, N. Sinclair, M. J. Stevens, A. E. Velasco, V. B. Verma, E. E. Wollman, S. Xie, D. Zhu, P. D. Hale, M. Spiropulu, K. L. Silverman, R. P. Mirin, S. W. Nam, A. G. Kozorezov, M. D. Shaw, K. K. Berggren, Demonstration of sub-3 ps temporal resolution with a superconducting nanowire single-photon detector, *Nature Photonics* 14 (2020) 250–255. doi:10.1038/s41566-020-0589-x. arXiv:1804.06839.
- [22] M. Perrenoud, M. Caloz, E. Amri, C. Autebert, C. Schönenberger, H. Zbinden, F. Bussièrès, Operation of parallel SNSPDs at high detection rates, *Superconductor Science Technology* 34 (2021) 024002. doi:10.1088/1361-6668/abc8d0.
- [23] I. Esmail Zadeh, J. Chang, J. W. N. Los, S. Gyger, A. W. Elshaari, S. Steinhauer, S. N. Dorenbos, V. Zwiller, Superconducting nanowire single-photon detectors: A perspective on evolution, state-of-the-art, future developments, and applications, *Applied Physics Letters* 118 (2021) 190502. doi:10.1063/5.0045990.
- [24] F. Martini, S. Cibella, A. Gaggero, F. Mattioli, R. Leoni, Waveguide integrated hot electron bolometer for classical and quantum photonics, *Optics Express* 29 (2021) 7956. doi:10.1364/OE.410317.
- [25] R. Cheng, Y. Zhou, S. Wang, M. Shen, T. Taher, H. X. Tang, A 100-pixel photon-number-resolving detector unveiling photon statistics, *Nature Photonics* 17 (2023) 112–119. doi:10.1038/s41566-022-01119-3.
- [26] A. Gaggero, F. Martini, F. Mattioli, F. Chiarello, R. Cernansky, A. Politi, R. Leoni, Amplitude-multiplexed readout of single photon detectors based on superconducting nanowires, *Optica* 6 (2019) 823. doi:10.1364/OPTICA.6.000823.
- [27] X. Hu, C. W. Holzwarth, D. Masciarelli, E. A. Dauler, K. K. Berggren, Efficiently Coupling Light to Superconducting Nanowire Single-Photon Detectors, *IEEE Transactions on Applied Superconductivity* 19 (2009) 336–340. doi:10.1109/TASC.2009.2018035.
- [28] F. Najafi, J. Mower, N. C. Harris, F. Bellei, A. Dane, C. Lee, X. Hu, P. Kharel, F. Marsili, S. Assefa, K. K. Berggren, D. Englund, On-chip detection of non-classical light by scalable integration of single-photon detectors, *Nature Communications* 6 (2015) 5873. doi:10.1038/ncomms6873. arXiv:1405.4244.
- [29] M. N. Notarnicola, M. G. A. Paris, S. Olivares, Hybrid near-optimum binary receiver with realistic photon-number-resolving detectors, *Journal of the Optical Society of America B Optical Physics* 40 (2023) 705. doi:10.1364/JOSAB.470806. arXiv:2207.07518.
- [30] M. Endo, T. Sonoyama, M. Matsuyama, F. Okamoto, S. Miki, M. Yabuno, F. China, H. Terai, A. Furusawa, Quantum detector tomography of a superconducting nanostrip photon-number-resolving detector, *Optics Express* 29 (2021) 11728. doi:10.1364/OE.423142. arXiv:2102.09712.
- [31] D. Peace, A. Zappacosta, R. Cernansky, B. Haylock, A. Boes, A. Mitchell, M. Lobino, Picosecond pulsed squeezing in thin-film lithium niobate strip-loaded waveguides at telecommunication wavelengths, *Journal of Physics: Photonics* 4 (2022) 035002. doi:10.1088/2515-7647/ac80e2.
- [32] F. Lenzi, J. Janousek, O. Thearle, M. Villa, B. Haylock, S. Kasture, L. Cui, H.-P. Phan, D. V. Dao, H. Yonezawa, P. K. Lam, E. H. Huntington, M. Lobino, Integrated photonic platform for quantum information with continuous variables, *Science Advances* 4 (2018) eaat9331. doi:10.1126/sciadv.aat9331.
- [33] M. Jönsson, G. Björk, Evaluating the performance of photon-number-resolving detectors, *Phys. Rev. A* 99 (2019) 043822. doi:10.1103/PhysRevA.99.043822.
- [34] K. Zou, Y. Meng, L. Xu, N. Hu, Z. Wang, X. Hu, Superconducting Nanowire Photon-Number-Resolving Detectors Integrated with Current Reservoirs, *Physical Review Applied* 14 (2020) 044029. doi:10.1103/PhysRevApplied.14.044029.
- [35] A. Engel, J. J. Renema, K. Il'in, A. Semenov, Detection mechanism of superconducting nanowire single-photon detectors, *Superconductor Science and Technology* 28 (2015) 114003. doi:10.1088/0953-2048/28/11/114003.
- [36] D. Sahin, A. Gaggero, Z. Zhou, S. Jahanmirinejad, F. Mattioli, R. Leoni, J. Beetz, M. Lerner, M. Kamp, S. Höfling, A. Fiore, Waveguide photon-number-resolving detectors for quantum photonic integrated circuits, *Applied Physics Letters* 103 (2013) 111116. doi:10.1063/1.4820842. arXiv:1308.4606.
- [37] D. E. Zelmon, D. L. Small, D. Jundt, Infrared corrected Sellmeier coefficients for congruently grown lithium niobate and 5 mol% magnesium oxide -doped lithium niobate, *Journal of the Optical Society of America B Optical Physics* 14 (1997) 3319–3322. doi:10.1364/JOSAB.14.003319.
- [38] V. Anant, A. J. Kerman, E. A. Dauler, J. K. W. Yang, K. M. Rosfjord, K. K. Berggren, Optical properties of superconducting nanowire single-photon detectors, *Optics Express* 16 (2008) 10750. doi:10.1364/OE.16.010750. arXiv:0806.3194.
- [39] A. Boes, L. Chang, M. Knoerzer, T. G. Nguyen, J. D. Peters, J. E. Bowers, A. Mitchell, Improved second harmonic performance in periodically poled LNOI waveguides through engineering of lateral leakage, *Optics Express* 27 (2019) 23919. doi:10.1364/OE.27.023919.
- [40] A. Boes, B. Corcoran, L. Chang, J. Bowers, A. Mitchell, Status and potential of lithium niobate on insulator (LNOI) for photonic integrated circuits, *Laser & Photonics Reviews* 12 (2018) 1700256. doi:10.1002/lpor.201700256.
- [41] L. Zhang, L. You, X. Yang, J. Wu, C. Lv, Q. Guo, W. Zhang, H. Li, W. Peng, Z. Wang, X. Xie, Hotspot relaxation time of nbn superconducting nanowire single-photon detectors on various substrates, *Scientific Reports* 8 (2018) 1486. doi:10.1038/s41598-018-20035-7.
- [42] Y. Meng, K. Zou, N. Hu, L. Xu, X. Lan, S. Steinhauer, S. Gyger, V. Zwiller, X. Hu, Fractal superconducting nanowires detect infrared single photons with 84% system detection efficiency, 1.02 polarization sensitivity, and 20.8 ps timing resolution, *ACS Photonics* 9 (2022) 1547–1553. doi:10.1021/acsp Photonics.1c00730.